sustainability

MDPI

Article

Research on Acquisition Performance of FFT Algorithm for Low-Frequency Spread-Spectrum Signals Using Acoustic Sensors

Yongzhuang Tang [1], Qidou Zhou [2], Zhiyong Xie [1], Wenxi Liu [1] and Xiaojun Lü [1,*]

[1] College of Naval Architecture and Ocean Engineering, Naval University of Engineering, 717 JieFang Road, Wuhan 430033, China; tang_yongzhuang@126.com (Y.T.)
[2] Ship Science Department, Naval University of Engineering, 739 JieFang Road, Wuhan 430033, China
* Correspondence: lvxj02@126.com

Abstract: An essential precondition for the effective use of low-frequency spread-spectrum acoustic signals is their synchronous acquisition. Due to the low bit rate that low-frequency spread-spectrum signals have, the length of the spreading spectrum code and the number of intra-chip carriers need to be precisely designed to balance the acquisition performance and the bit rate in low-frequency spread-spectrum signals. Furthermore, the selection of the acquisition method and sampling frequency depends on the specific application and system requirements, which will directly affect the processing speed and accuracy. Firstly, this study uses a cyclical stepping search combined with a fixed threshold and maximum correlation discriminant method to improve the FFT acquisition algorithm with a low Doppler frequency. Secondly, the effects of the spreading spectrum code parameters and sampling frequency on the acquisition performance are also investigated through simulation and experiments with acoustic sensors. The results show that both lengthening the spreading spectrum code and increasing the number of intra-chip carriers can greatly improve the acquisition performance. Increasing the sampling frequency can improve the ranging accuracy but has a very limited improvement effect on the acquisition performance.

Keywords: acoustic sensors; low-frequency spread-spectrum acoustic signals; FFT acquisition algorithm; the number of intra-chip carriers; the length of spreading spectrum code

Citation: Tang, Y.; Zhou, Q.; Xie, Z.; Liu, W.; Lü, X. Research on Acquisition Performance of FFT Algorithm for Low-Frequency Spread-Spectrum Signals Using Acoustic Sensors. *Sustainability* **2023**, *15*, 6405. https://doi.org/10.3390/su15086405

Academic Editors: Tan Yigitcanlar and Fadi Al-Turjman

Received: 7 February 2023
Revised: 20 March 2023
Accepted: 6 April 2023
Published: 9 April 2023

1. Introduction

Spread-spectrum modulation is a widely used application in radio communication [1,2] and global navigation satellite systems (GNSS) [3,4] due to its excellent anti-interference and high processing gain. Free from the contradiction between ranging accuracy and distance ambiguity faced by conventional pulse signals, spread-spectrum signals are also applied to radar detection [5], and air ultrasonic detection and perception [6–8]. In response to the growing civil and military needs for underwater communication and detection, the spread-spectrum method has been introduced into underwater acoustic signal treatment to cope with the complex and changeable marine environment [9]. The key step to realizing the effective utilization of spread-spectrum signals is their accurate acquisition [2]. Differing from radio and ultrasonic spread-spectrum signals, underwater acoustic signals generally use relatively lower frequencies ranging from several thousand hertz to several hundred hertz, depending on the specific application and environmental factors. In particular, for long-distance transmission, the frequency of underwater acoustic signals is required to be below 1000 Hz and even below 500 Hz [10]. Additionally, underwater acoustic low-frequency signals have limited available bandwidth and a low bit rate [11]. The length of spreading spectrum codes and the number of carriers in a chip directly determine the bit rate, which, in turn, affects the acquisition performance. In addition, the acquisition

method will affect the accuracy and speed of the acquisition, which will further affect the performance of the spread-spectrum system in specific applications.

Spread-spectrum signal acquisition, in essence, is the identification of the correct code phase and carrier Doppler in signals that are received through two-dimensional searches in both the time and frequency domains by taking advantage of the excellent autocorrelation properties of the spreading spectrum codes [12]. Early spread-spectrum signal acquisition methods typically relied on time-domain sliding correlation, sequence estimation searches, and the matched-filter technique, which gradually improved the search efficiency. The FFT method, proposed by Grant [13,14], enabled the code phase search using one operation, truly achieving a parallel search in the time domain. Huang [15] proposed a modified PMF-FFT acquisition algorithm to improve the accuracy of the Doppler frequency offset estimation. The authors of [16] used an improved FFT circular correlation scheme with circular shifts in the frequency domain, which performed all frequency searches within a preset range by cyclically shifting the signal FFT results and delivered higher computational efficiency than conventional algorithms. Nonetheless, the scheme employed a fixed step size to compute all frequencies within the estimation range, which resulted in many invalid frequency searches [17]. The frequency search range had to be preset, and at least two times the expected maximum Doppler frequency was required to provide enough margin of error. However, there was still a trade-off between the search range and capture speed depending on the particular application and requirements. Moreover, following the maximum discrimination acquisition, the scheme fed back the phase and Doppler of the maximum values of the correlation upon the completion of a full search regardless of whether the acquisition was accurate and whether there were desired signals. To address these problems, this paper combines the fixed threshold and maximum discrimination methods to discriminate the acquired results, so as to integrate their advantages while making up for their drawbacks. Using a low-frequency spread-spectrum signal with a low Doppler frequency, the frequency circular shift search method changes the traversal search to the step-by-step search in the preset range, thereby avoiding excessive invalid searches and the difficulty in setting the search range.

Since radio spread-spectrum carriers are radio frequency carriers with a high code rate, long spreading spectrum codes, such as the GPS C/A code as a 10-order sequence [3], are generally directly used to boost performance. In the field of GNSS, abundant research has been conducted on spreading spectrum code design, but much is concentrated on designing pseudo-code sequences with a better performance and new design methods, exemplified by the Kasami code and Weil code derived from the conventional sequences [18,19]. Sun et al. [20] studied the influence of the change of the partial matched filter length on the acquisition performance indexes. Hussain [21] proposed a new adaptive data length (ADL) method for acquisition to speed up the acquisition process. In general, the selection of parameters such as the length of the spreading spectrum codes may not be the focus of GNSS. However, low-frequency spread-spectrum signals cannot accept unduly long spreading spectrum codes. Consequently, designing spreading spectrum codes with an appropriate sequence length and intra-chip carriers with a reasonable number turns out to be the key to ensuring the desired bit rate and acquisition performance. Furthermore, the sampling frequency determines the volume of data, and thus choosing an appropriate sampling frequency can balance the performance and the processing efficiency.

With the improved FFT acquisition algorithm, this paper mainly explores the influence of the spreading spectrum code parameters and sampling frequency on the acquisition performance through simulation and experiments. The real underwater environment is so complex that it is difficult to conduct extensive experiments, and the law of a single parameter is easily disturbed by unknown factors. Hence, the acoustic sensor is used to conduct experiments in the air, where, in addition to convenient experimental operations and controllable environmental conditions, the difference between the acoustic media will not significantly change the effect of the parameters themselves on the acquisition performance.

2. Improved FFT Acquisition Algorithm

2.1. Fuzzy Function and 2D Search Step Size

The received spread-spectrum signal can be written as:

$$s(t) = Ad(t-\tau)x(t-\tau)\cos(2\pi(f_c + f_D)t + \theta) + n(t) \tag{1}$$

where A is the amplitude of useful signals, d is the information code, which is considered to be constant 1 or -1 in the acquisition range, x is the spreading spectrum code, τ is the spreading spectrum code phase, f_c is the transmit carrier frequency, f_D is the Doppler frequency, θ is the carrier phase, and $n(t)$ is the noise.

$$\exp[-j(2\pi(f_c + \hat{f}_D)t + \hat{\theta})] \tag{2}$$

The received signal is multiplied by the two locally generated orthogonal carriers (Equation (2)) so that carrier stripping can be achieved after it passes through a low-pass filter. For the sake of simplicity, the noise term is omitted and the equation can be rewritten as:

$$Ad(t-\tau)x(t-\tau)\exp j(2\pi\Delta f_D t + \Delta\theta) \tag{3}$$

where $\Delta\theta$ is the difference between the actual phase of the received carrier and the estimated carrier phase, and f_D is the difference between the actual Doppler and the estimated Doppler of the local carrier. In practical acquisition algorithms, if a Doppler and carrier phase cannot be initially estimated, $\hat{f}_D$ and $\hat{\theta}$ are usually set to zero and then related with the locally generated spreading spectrum code:

$$\widetilde{S} = Ad\exp(j\Delta\theta) \times \frac{1}{T_s}\int_0^{T_s} x(t-\tau)x(t-\hat{\tau})\exp(j2\pi\Delta f_D t)dt \tag{4}$$

where T_s is integration time. The fuzzy function is defined as:

$$R(\Delta\tau, \Delta f_D) = \frac{1}{T_s}\int_0^{T_s} x(t-\tau)x(t-\hat{\tau})\exp(j2\pi\Delta f_D t)dt \tag{5}$$

When the Doppler frequency estimation error is zero, Equation (5) can be written as an autocorrelation function of the spreading spectrum code:

$$R(\Delta\tau) = \begin{cases} \frac{N+1}{N}\frac{\Delta\tau}{T_c} + 1 & , -T_c < \Delta\tau < 0 \\ -\frac{N+1}{N}\frac{\Delta\tau}{T_c} + 1 & , 0 < \Delta\tau < T_c \\ -\frac{1}{N} & , \text{otherwise} \end{cases} \tag{6}$$

where N is the code length. According to the characteristics of the autocorrelation function, a relatively obvious correlation peak will appear only when the phase difference is less than one chip, thereby attaining chip synchronization.

If the chips are completely aligned, Equation (5) can be rewritten as:

$$R(\Delta f_D) = \exp(j2\pi\Delta f_D T_s)\text{sinc}(\pi\Delta f_D T_s) \tag{7}$$

Figure 1 is a frequency fuzzy search function. From the positions of the zero points of the curves in the figure and the period of the sinc function, the maximum step size of the Doppler search can be determined to be $1/T_s$. As can be seen, the longer the integral time, the smaller the Doppler search step size and the higher the accuracy, and hence, the more search time and resources consumed. Noteworthily, the conclusion that the longer the integral time, the higher the frequency search accuracy is drawn from the perspective of the maximum search step size, which does not mean that the highest frequency accuracy can only reach $1/T_s$.

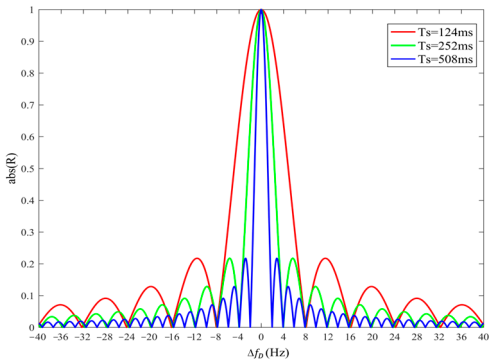

Figure 1. Doppler search fuzzy function for different integral times.

The longer the integral time, the sharper the correlation peak, and the better the frequency resolution. When the integral time is constant, a search step longer than $1/T_s$ is prone to miss the signal peaks and the failure of correct acquisitions. The smaller the search step size, the more likely the search frequency falls on the signal peak.

2.2. Conventional FFT Acquisition Methods

Conventional FFT acquisition methods are divided into time-domain parallel/frequency-domain serial acquisitions and frequency-domain parallel/time-domain serial acquisitions. Time domain parallelism means that all code phases can be searched through one FFT, and the process is shown in Figure 2.

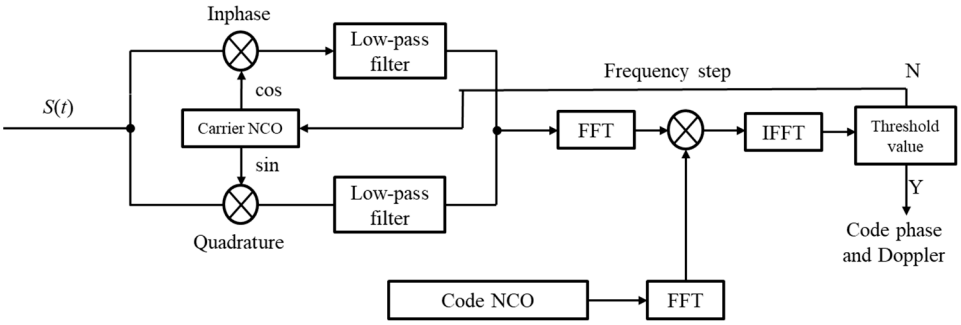

Figure 2. FFT time-domain parallel/frequency-domain serial acquisition algorithm.

Although the time-domain parallel FFT method requires a greatly reduced number of integration times compared with the typical time-domain serial methods, the serial search is still necessary for frequency. Consequently, for each frequency domain, one FFT and one IFFT should be conducted. Moreover, in order to improve the frequency search accuracy, the measures available only include increasing the integral time and reducing the step size of the search, leading to a lack of consideration of both the accuracy and efficiency. In addition, the probability of acquisition according to the discrimination threshold alone is greatly affected by noise. If the threshold value is set too large, it is likely to result in missing a correct acquisition. In contrast, if the value is set too small, the probability of false alarms will rise. An adaptive threshold will increase the complexity of the system. The frequency-domain parallel/time-domain serial FFT search method also faces similar problems, in addition to a large number of invalid frequency searches.

2.3. FFT-Based Circular Shift Fast Acquisition Algorithm Combining Maximum Correlation and Threshold Discrimination

The frequency circular shift method achieves the frequency search function of conventional FFT methods by utilizing the shift of the input signal's FFT result. Hence, the problem of the need for multiple FFT operations in the frequency serial search is addressed.

For K frequency searches, conventional FFT algorithms need to perform K FFT operations and K IFFT operations. However, if the frequency circular shift method is employed, only FFT operations and K IFFT operations are needed for the input signal. Since the data in the shift operations have been pre-stored, the increased shift operation time is much lower than the reduced FFT operation time. Nonetheless, the frequency circular shift requires a preset range and the traverse calculation of each frequency. The result of the maximal value decision method faces the problem of whether or not the correct acquisition has been obtained.

As shown in Figure 3, the carrier stripping process of the signal can be replaced by multiplying the local spreading spectrum code by the local carrier, and the frequency shift can be achieved by shifting the FFT frequency domain result of the local spread-spectrum signal. Each time the FFT frequency domain result is shifted once, the spectrum is shifted by exactly one maximum search Doppler (1/Ts). In contrast to the frequency circular shift method in Ref. [16], the improved method judges the acquired result after each shift, dispensing with the calculation for all of the frequencies within the preset range. At the same time, the maximum range of the step-by-step search is twice the estimated maximum Doppler. However, due to the absence of the traversal frequency, the correct code phase and Doppler cannot be obtained at the same time only through maximum discrimination. Hence, a threshold can be set to avoid searching for sidelobe frequencies, and the combination with the maximum correlation during the acquisition discrimination can improve its acquisition capability. The main purpose of setting a threshold is to ensure that the frequency search enters the main peak rather than serving as the basis for a successful acquisition. Only when the minimum threshold is exceeded, the phase and Doppler of the maximum output code will be selected, which therefore avoids the false feedback in the case of no signal and a small signal-to-noise ratio. Therefore, the threshold needs only to be higher than the sidelobes of the correlation peak in Figure 1. As shown by the dotted lines in Figure 3, a more accurate Doppler can be acquired within the main peak range. Since the range of fine searches is small, it will not cause too much computational burden.

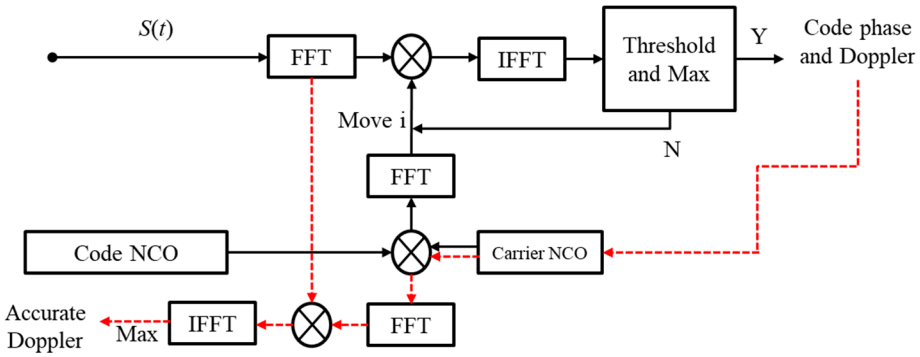

Figure 3. Circular shift FFT method combining maximum correlation and threshold discrimination.

3. Simulation Analysis of Factors Affecting Algorithm Performance

3.1. Effect of Spread-Spectrum Signal Waveform Parameters

In order to study the effect of the code length, the carrier and sampling frequencies are set to 1000 and 16,000 Hz, respectively, and there are four carrier cycles in each chip. A total of 5000 Monte Carlo simulations are performed for each working condition, and the acquisition success probability is calculated for the different code lengths and different numbers of intra-chip carriers. In the simulation, the true code phase difference and Doppler are known, and the correctness and accuracy of the capture can be judged by comparing them with the acquisition results. The influence of the parameters on the acquisition performance can be characterized by simulating the acquisition probability under different signal-to-noise ratios.

As illustrated in Figure 4a, as the code length increases, the integral time T_s increases by the same factor, and the acquisition performance under a low SNR is significantly boosted. This is because an increasing integral length leads to a higher correlation peak and a larger possibility of successfully extracting useful information from the noise. Furthermore, the acquisition success probability is calculated under the conditions that the code length $N = 63$ and there are two carriers in each chip ($T_s = 126$ ms). The calculated integral time is very close to that calculated using $N = 31$, and the acquisition probabilities in the two cases are not much different either. This suggests that under a constant sampling frequency, only increasing the code length cannot remarkably improve the acquisition performance if the integral time remains unchanged. If the number of carriers in a chip remains unchanged (T_c is constant), lengthening the spreading spectrum code will increase the integral time and thus significantly enhance the acquisition performance. In low-frequency signals, only a limited number of carriers can be used within a chip so as to ensure the bit rate and bandwidth. The larger the number of intra-chip carriers, the wider the chip and the smaller the bandwidth. The simulation results in Figure 4b show that within a certain SNR range, the acquisition probability is significantly raised and the acquisition performance improved as the number of carriers in the chip increases.

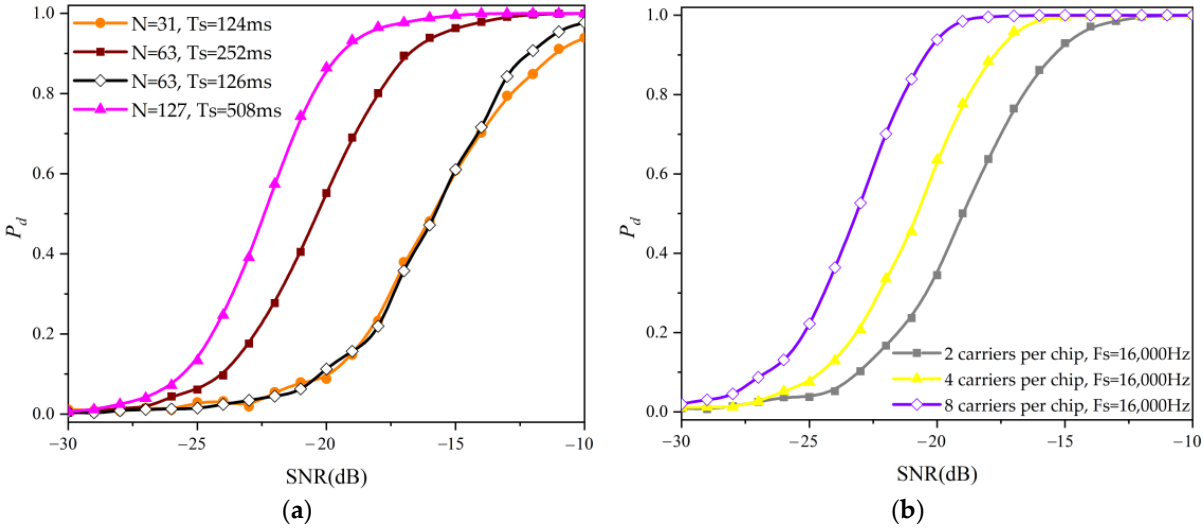

Figure 4. Effects of different spreading spectrum code parameters on acquisition success probability: (**a**) Different spreading spectrum code lengths N; (**b**) Different numbers of carriers in a single chip.

3.2. Effect of Sampling Frequency

The fixed spreading spectrum code length $N = 63$, the carrier frequency $f_c = 1000$ Hz, and there are four carriers in one chip (chip length $T_c = 4$ ms). For the received signal, the chip phase $\Delta\tau = 30$ chips and the Doppler $f_D = 1$ Hz. The variation in the acquisition probability with the signal-to-noise ratio (SNR) is calculated under four different sampling frequencies. At each sampling frequency, 5000 Monte Carlo simulations are performed. An acquired result with a chip error not exceeding 0.2 chips and a carrier frequency error less than 0.5 Hz is identified as a successful acquisition, and based on this, the corresponding successful acquisition probability P_d is calculated.

As shown in Figure 5, as the sampling frequency increases, the probability of correct acquisition rises. Furthermore, as can be seen in Figure 6, the noise-induced sidelobe peaks increase with the decreased SNR and there is no evident maximum correlation peak, which leads to the failure of correct acquisitions. Increasing the sampling frequency can increase the value of the maximum correlation peak and suppress the height of the sidelobes, which indicates that a reasonable increase in the sampling frequency contributes to an increasing acquisition probability.

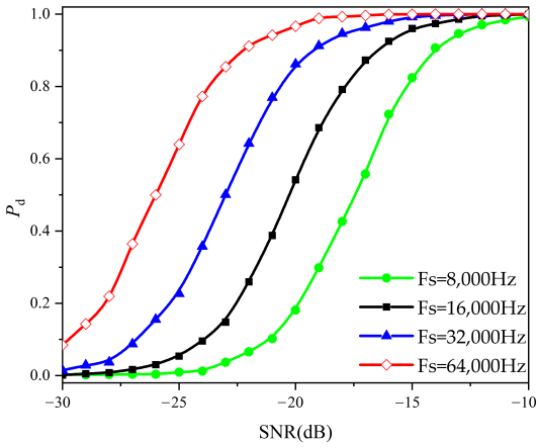

Figure 5. Acquisition success probabilities at different sampling frequencies.

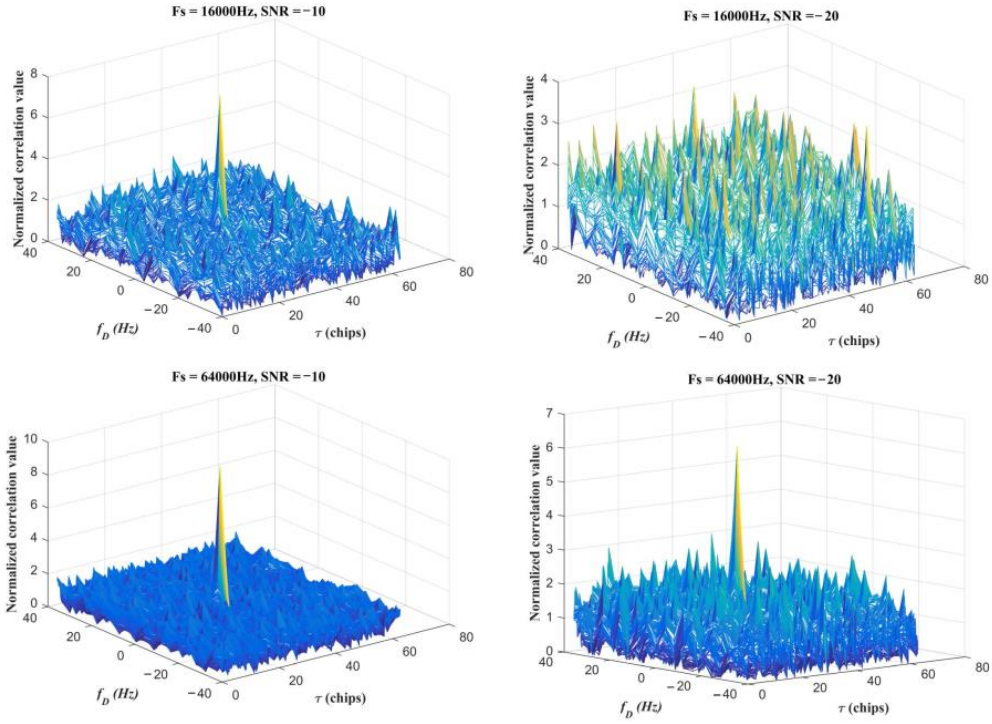

Figure 6. Correlation values at different sampling frequencies and SNR.

4. Experimental Verifications

4.1. Accuracy Verification of Improved FFT Acquisition Algorithm

In order to verify that the accuracy of the algorithm and the acquired signal is indeed the desired signal, the spread-spectrum signal reception experiment is carried out in a closed room with a multipath environment where there is natural reverberation and mechanical noise from the signal transmission and acquisition system. The experimental layout is shown in Figure 7. As illustrated, the woofer for the signal acquisition is located directly in front of the sound source and has a distance of 191.0 cm away from the front wall. The speed of sound in air is 340 ms^{-1}. The transmit signal is a spread-spectrum signal containing the bit information, with the spreading spectrum code length of $N = 63$, the chip width $T_c = 4$ ms, and the carrier frequency of 1000 Hz. The sampling frequency is set to 16 kHz. Considering that it is only for testing the acquisition performance, the data acquisition time is set to 20 s, which is enough to satisfy the requirement for signal length. Two groups of experiments with high signal-to-noise ratios and low signal-to-noise

ratios are adopted. When the correlation peak exceeds the threshold, the acquisition can be achieved. By comparing the time delay difference of the captured reflected signal with the theoretical time delay calculated by the real reflected path, the code phase accuracy of the captured signal can be further judged. As shown in Figure 8, the power of the background noise individually measured is concentrated at 281 Hz, and the peak in the power spectrum is 50.80 dB; the power peak at the center frequency of the measured signal in the background noise environment is 49.86 dB. In the white noise environment, the signal power is much lower than the noise power.

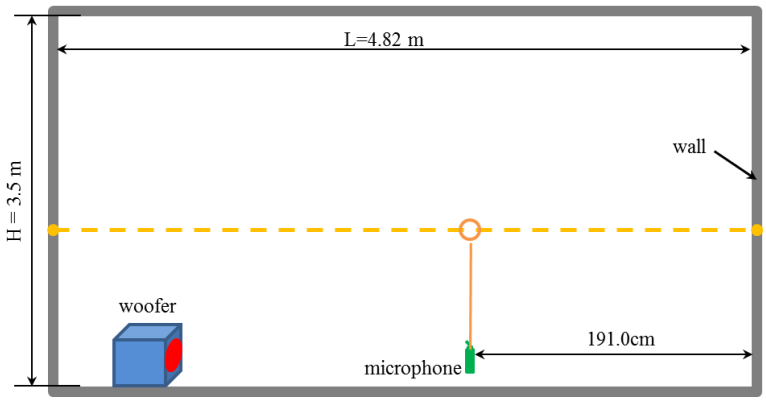

Figure 7. Experimental layout.

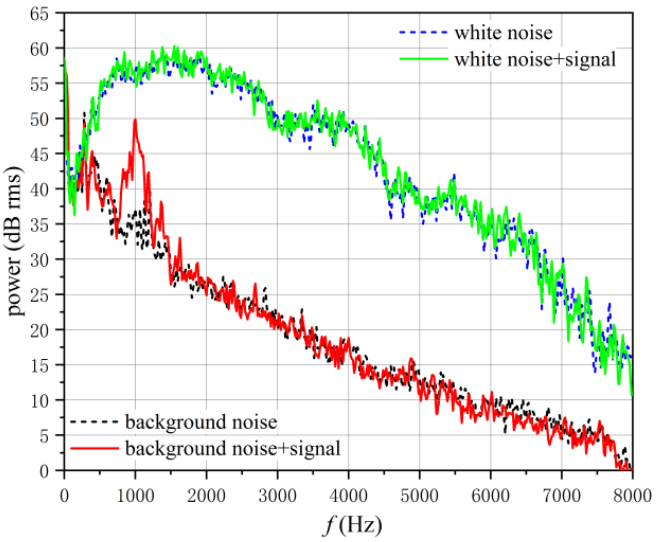

Figure 8. Noise and signal power spectrum.

As can be seen in Figure 9a, the proposed algorithm can satisfactorily acquire the spread-spectrum signals that have a peak power equivalent to that of the background noise; there are two obvious correlation peaks in the acquired result, of which the relatively low correlation peak is thought to be caused by the signal reflected from the front wall. The time delay difference between the reflected signal captured and the direct signal is 2.828 chips, and the theoretical difference is 2.809 chips. The distance between the woofer and the front wall calculated from the time delay difference in the spread-spectrum signal is 192.3 cm, and the experimental error is only 1.3 cm. Hence, the errors in the time delay difference and distance are both much smaller than the theoretical errors (0.5 chip and 68 cm, respectively) in spread-spectrum signal ranging. This indicates that the acquisition algorithm can not only correctly acquire the code phase and Doppler, but also achieve a high acquisition accuracy and ranging accuracy. Since there are many sampling points

in one chip, the time of arrival of the signal can be determined more accurately using maximum correlation discrimination. Although the correlation peak width exceeds one chip, the maximum discrimination method can, to a large extent, overcome the ambiguous error within the chip.

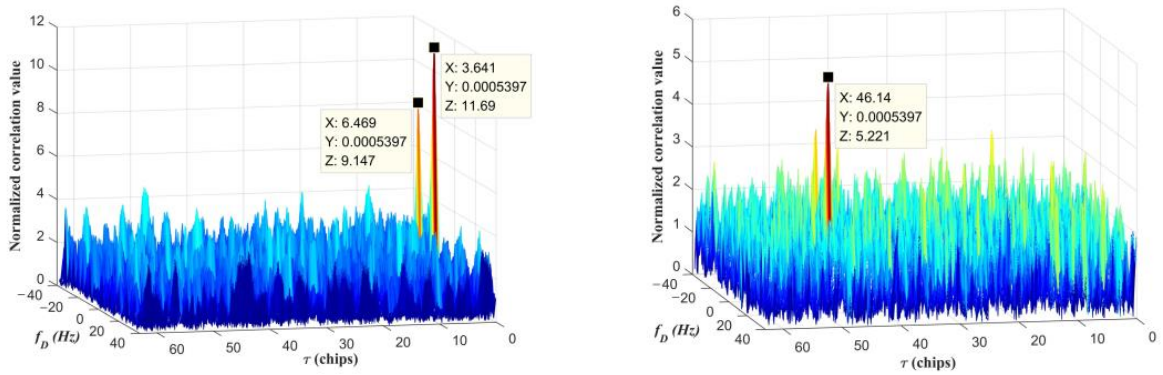

Figure 9. Acquired results: (**a**) Acquired result with background noise; (**b**) Acquired result with background noise + white noise.

Since the power of the background noise is concentrated in a small low-frequency range, further interference is applied to simulate wideband white noise by playing white noise externally with the power of the transmitted signal remaining unchanged. Figure 8 shows the measured white noise and signal power spectrum. The noise power near the signal carrier frequency has far exceeded the measured signal power of the ambient noise, and the signal power spectrum of the white noise is almost the same as when there is only white noise; that is, the signal has been completely submerged in the noise. As shown in Figure 9b, the correlation peaks of the direct signals are still very obvious and can be acquired, while only the weak reflected signals are covered up by the noise. Although there are some relatively high sub-peaks, an accurate acquisition can still be achieved by combining the threshold discrimination and maximum correlation acquisition methods. If only the threshold discrimination method is used, problems including high false alarm probability or a low detection rate will occur.

4.2. Verification of the Effects of Spread-Spectrum Signal Waveform Parameters and Sampling Frequency on Acquisition Performance

In order to further investigate and verify the effects of the spread-spectrum signal waveform parameters and sampling frequency on acquisition performance, 11 cases of comparative experiments are designed, as shown in Table 1. Each experiment is conducted in the same environment with the white noise externally applied, and the positions of the sound source and woofer are fixed. The carrier frequency of the transmit signal is 1000 Hz, the waveform amplitude of the original signal is 0.5 V, and the power of the amplifier remains unchanged. The length of the spreading spectrum code of the transmit signal N, the number of carriers in each chip (equivalent to T_c), and the sampling frequency F_s are changed separately to receive signals and acquire the FFT. The effects of the parameters on the acquisition performance are measured by whether or not an accurate acquisition is achieved and the relative peak value of the normalized correlation curve. The normalized correlation value represents the ratio of the correlation value at the sampling point to the average correlation value in the time period of integration. To a certain extent, a higher normalized correlation peak value suggests a better anti-noise performance and easier achievement of the acquisition.

Table 1. Parameters of spread-spectrum signals in different cases.

Case	Code Length N	No. of Intra-Chip Carriers	T_c	T_s	Sampling Frequency F_s
1	31	4	4 ms	124 ms	16 kHz
2	63	4	4 ms	252 ms	16 kHz
3	127	4	4 ms	508 ms	16 kHz
4	63	2	2 ms	126 ms	16 kHz
5	63	8	8 ms	504 ms	16 kHz
6	63	16	16 ms	1008 ms	16 kHz
7	31	16	16 ms	496 ms	16 kHz
8	63	4	4 ms	252 ms	2 kHz
9	63	4	4 ms	252 ms	4 kHz
10	63	4	4 ms	252 ms	8 kHz
11	63	4	4 ms	252 ms	32 kHz

In the Table 1, Cases 1, 2, and 3 are used to compare the effect of the code length N on the acquisition performance; Cases 2, 4, 5, and 6 are used to investigate the variations in the number of carriers in each chip; and Cases 2, 8, 9, 10, and 11 are used to explore the effect of the sampling frequency on the acquisition performance. In Cases 3, 5, and 7, N and T_c vary, but the duration T_s of their spreading spectrum codes is almost the same. Since T_s is dependent on N and T_c, these three cases can be used to study the effect of T_s.

For the power spectra of the signals and noise in the first case, there is no obvious peak at 1000 Hz, and the spread-spectrum signals have been basically submerged in white noise. Figure 10 shows the power spectrum of the noise and received signal in the first case. The effect of each parameter on the anti-noise performance of the acquisition algorithm can be studied through the results acquired using different parameters.

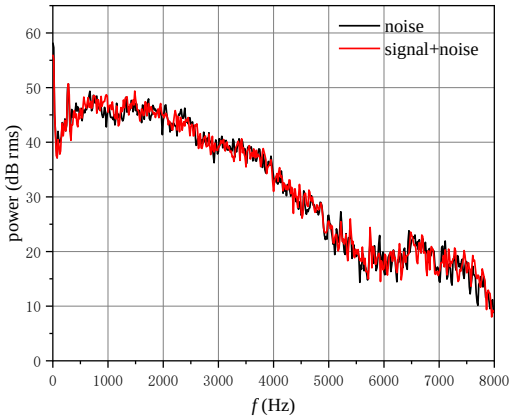

Figure 10. Noise power spectrum and received power spectrum of spread-spectrum signal (Case 1).

4.2.1. Spread-Spectrum Signal Waveform Parameters

According to the results in Figure 11, the spread-spectrum signals with different code lengths N are all acquired, and the time delay difference between the two peaks also verifies the correctness of the acquired results from the side. In Figure 11a, although the acquisition can be achieved at N = 31, there is a lot of noise and multipath-induced peaks. As long as the noise is slightly higher, the direct signal correlation peak may be submerged, making it difficult to acquire. From the size of the normalized correlation value of the direct signal, the longer the code length, the more obvious the correlation peak, and the better the anti-noise performance. Accordingly, the acquisition performance is higher, with an improved probability of acquisition. This is consistent with the simulation result, i.e., the larger the code length N, the higher the acquisition probability.

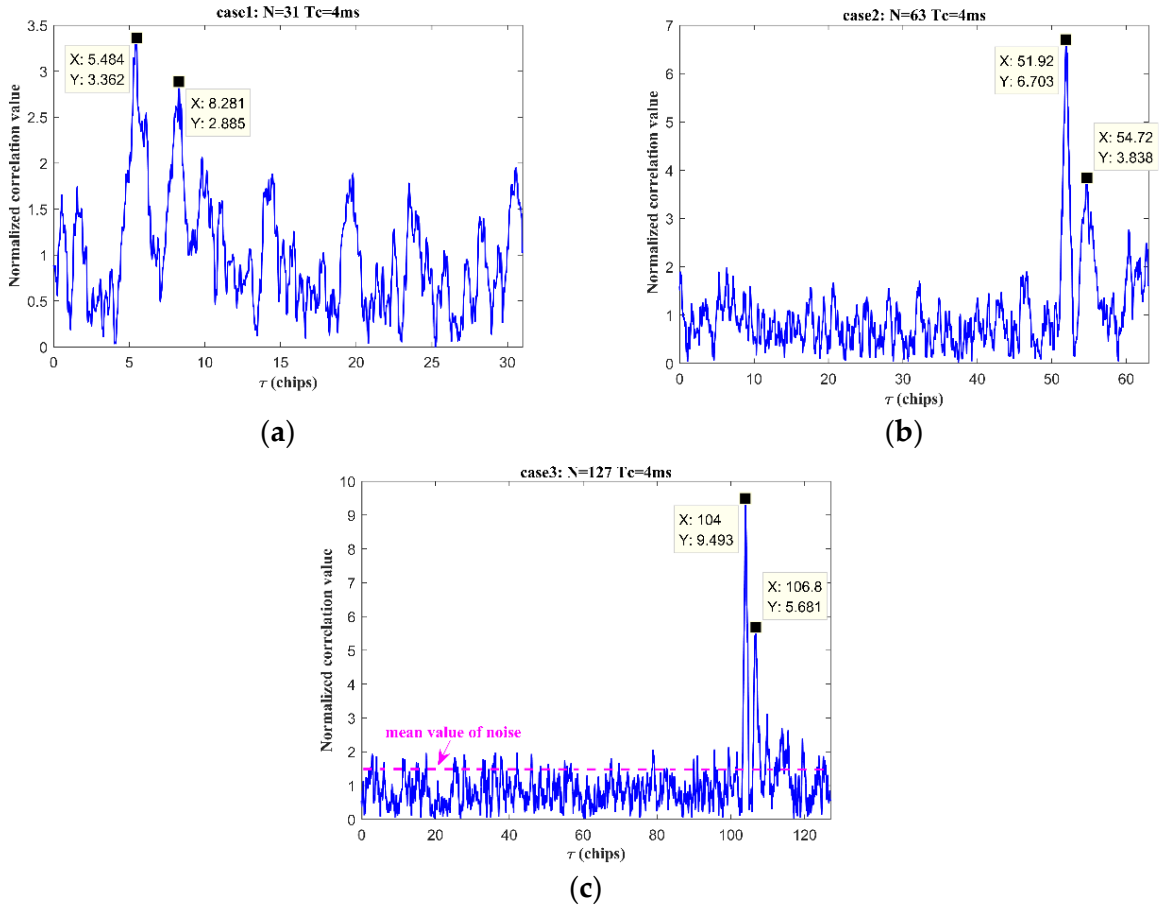

Figure 11. Acquired results for spread-spectrum signals with different code lengths N: (**a**) Case 1, N = 31; (**b**) Case 2, N = 63; (**c**) Case 3, N = 127.

Figure 12a shows that the acquisition performance is poor when the number of intra-chip carriers is 2. It can be seen from the correlation curve that despite a maximum peak, the height of the sidelobe in the noise is high, and thus the anti-noise performance is poor. The comparison of Figures 12a–c and 11b reveals that as the number of carriers in the chip rises, accurate acquisitions are achieved, and the height of the normalized correlation peak increases accordingly. Hence, increasing the number of intra-chip carriers alone results in an improvement in the acquisition performance, as also found in the simulation. The comparison of Figure 12b,d and Figure 11c shows that the spread-spectrum signals in the three cases have almost the same Ts, but vary in the code length N, and the number of intra-chip carriers. In addition, the normalized correlation peak heights of the direct signals in the three cases are found to vary greatly, and the higher the code length, the higher the peak. This contrasts with the simulation result that similar Ts values lead to approximately the same acquisition probability. A further comparison reveals that the ratios of the height of the maximum normalized correlation peak to the mean value of the background (noise) in the three cases are 6.88 (Case 7), 6.20 (Case 5), and 6.12 (Case 3), respectively. Given the similarity of the three values, it is safe to think that the signals in these three cases have a similar anti-noise performance. The value of the normalized peak in Figure 12d, for example, is small. This should be ascribed to the interaction between the multipath signals when the number of intra-chip carriers and the width of the chip are large, which enhances the absolute sizes of the main peak of the direct signal and the sidelobes of the other signals. In this example, the length of the spreading spectrum code is short and the main peak occupies a large proportion of the time domain, which significantly increases the average correlation value in the code period and makes the normalized value of the main peak unduly small. The unduly large ratio of the peak value to noise mean value in Case 7 is

also due to the substantial improvement in the anti-noise performance due to the multipath effect. It should be pointed out that for the correlation analysis above, the change of a single variable still does not result in a loss of accuracy when using the normalized correlation value to measure the anti-noise performance of the acquisition method. In general, the three cases vary greatly in the code length and the number of carriers but have almost the same Ts. The acquisition method using the maximum correlation discrimination delivers a similar acquisition performance for the signals in the three cases, and the performance is dominated by Ts. If the threshold discrimination method is employed, the broadening of the correlation peak and sub-peak enhancement in Figure 12d tend to cause false alarms and inaccurate acquisition results.

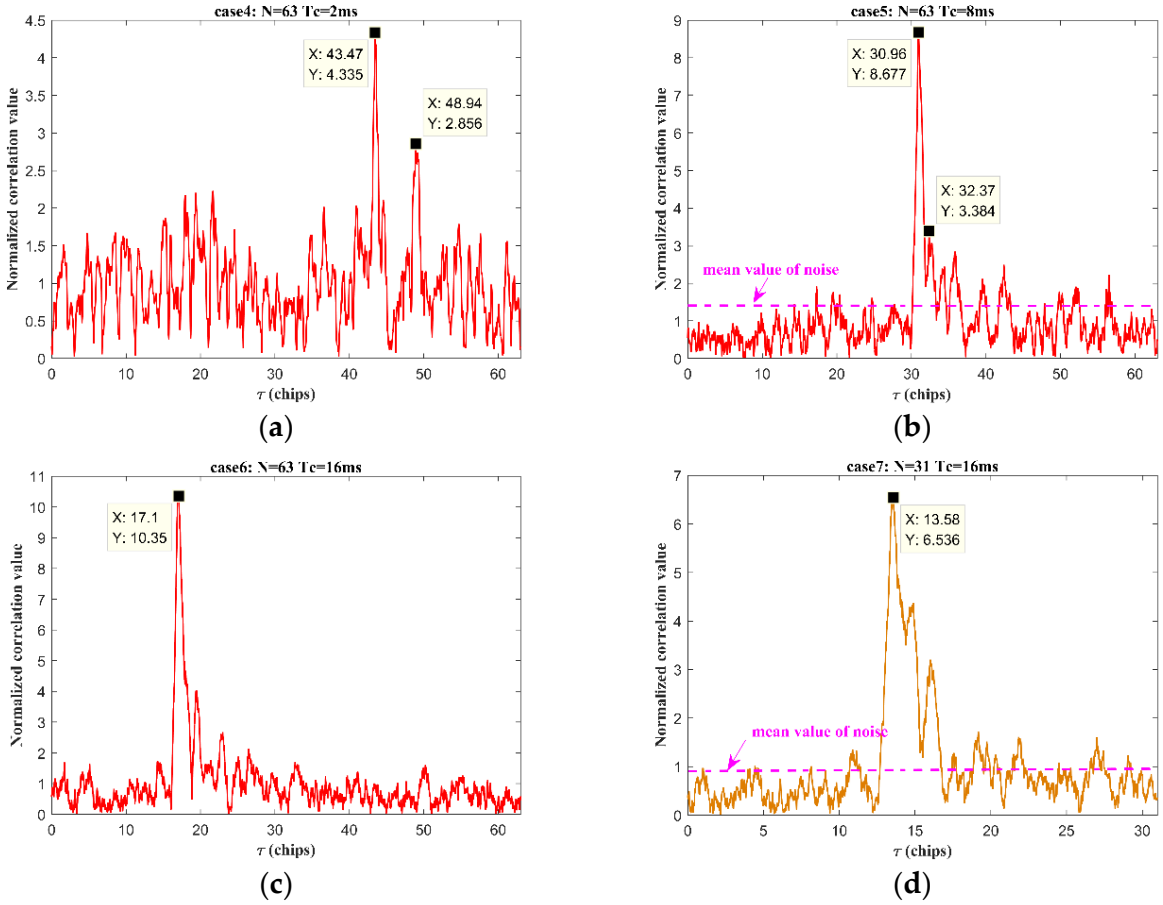

Figure 12. Acquisition correlation curves at different numbers of intra-chip carriers: (**a**) Case 4, 2 carriers per chip; (**b**) Case 5, 8 carriers per chip; (**c**) Case 6, 16 carriers per chip; (**d**) Case 7, 16 carriers per chip (N = 31).

The analysis above shows that increasing the code length N and the number of intra-chip carriers separately can both enhance the signal correlation and increase the acquisition performance. Since the length N and the number of intra-chip carriers jointly determine the length Ts of the spreading spectrum code periodic signal (the integral time length of the correlation calculation), the length of the integral time is an inherent main factor affecting the correlation performance. Although widening the chip reduces the bandwidth, adverse effects may be caused in the performance of the spread-spectrum system. However, the experiments show that in a white noise environment, the bandwidth reduction within a certain range does not offset the benefits brought by the increase in the integral length to the acquisition performance. In the case of multipath reverberation, for a fixed threshold for discrimination, an excessively wide chip may broaden the correlation peak, resulting in a low capture accuracy and false alarms. At this moment, it is better to increase N. For

maximum discrimination, the gain of the main peak correlation value produced by the multipath action has certain benefits for the improvement of the acquisition performance.

4.2.2. Sampling Frequency

The five correlation curves in Figures 11b and 13 are compared. The sampling frequency is twice the carrier frequency, following the sampling theorem. Although the largest correlation peak is identified, there are many sub-peaks in the correlation curves, and thus the anti-noise performance is poor. As the sampling frequency is gradually raised, the correlation peak is slightly increased, and the anti-noise performance is improved. If the sampling frequency is continuously increased, after exceeding 8 kHz, the improvement is far inferior to that achieved by increasing N or increasing the number of intra-chip carriers, and the correlation value even decreases at 32 kHz. These findings indicate that increasing the sampling frequency does not significantly increase the acquisition performance in practice. In the Gaussian white noise channel simulated in Section 3.2, the original waveform is only superimposed with noise, and more information that strictly contains the original waveform can be extracted if enough sampling points are employed. The correlation calculation can suppress the noise to achieve the acquisition. Since the signal waveform actually transmitted through the real channel (including multipath reverberation) has been distorted, an unduly high sampling frequency cannot sufficiently restore the original waveform and extract more accurate information, which therefore leads to the failure in improving the correlation performance. The experimental results show that it is better to use 8–16 times the carrier frequency as the sampling frequency. In practical applications, a reasonable sampling frequency can be adopted, and a sufficient gain cannot be expected to be obtained by increasing the sampling frequency.

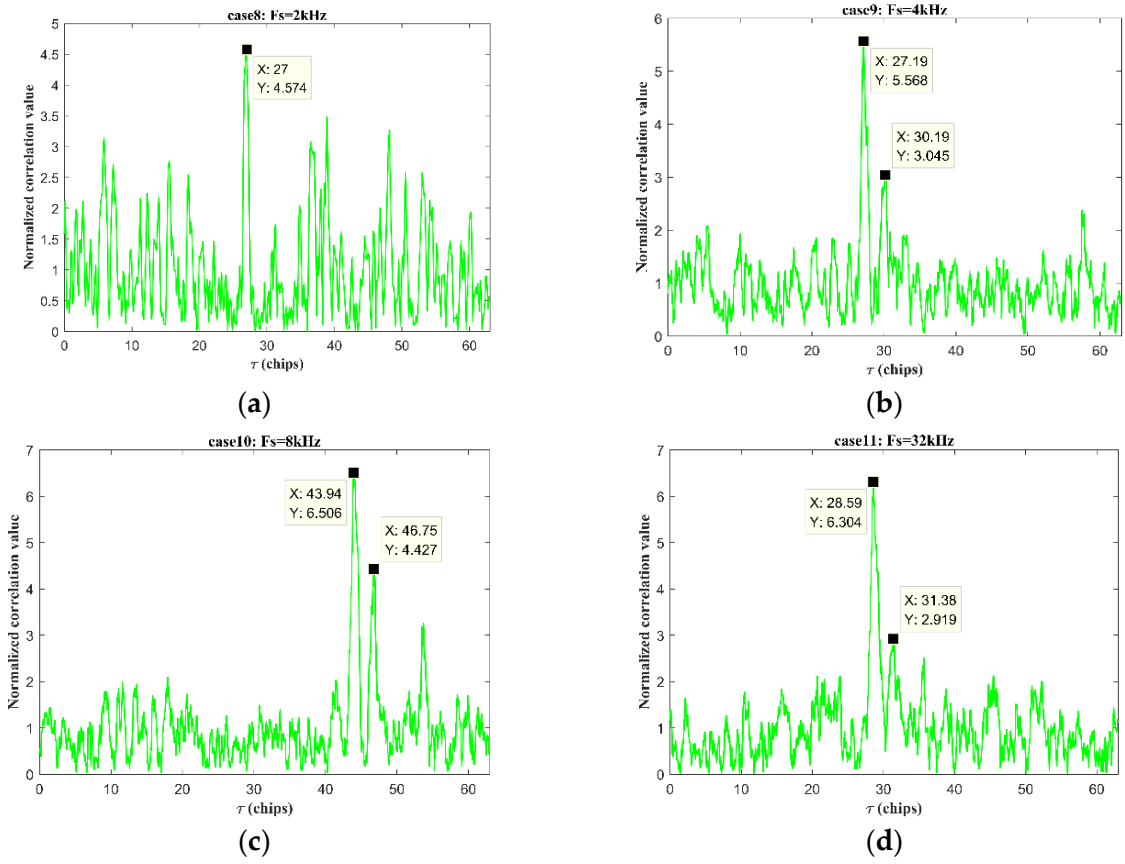

Figure 13. Acquisition correlation curves at different sampling frequencies: (**a**) Case 8; (**b**) Case 9; (**c**) Case 10; (**d**) Case 11.

In addition, the results in Figures 11b and 13 show that the sampling frequency has a certain influence on the phase precision of the acquisition code. When the sampling frequency is 4 kHz, the time delay measurement error between the direct signal and the reflected signal is 0.2 chip (0.001 chip at 8 kHz, 0.018 chip at 16 kHz, and 0.019 chip at 32 kHz). It can be seen that increasing the sampling frequency appropriately can improve the accuracy of the acquisition and ranging.

5. Conclusions

The improved FFT acquisition algorithm increases the acquisition performance by combining the fixed threshold and maximum correlation discrimination methods. The selection of an appropriate sequence length and intra-chip carriers is critical to the design of the spreading spectrum codes. These parameters can impact the performance and efficiency of the system. Thus, acoustic sensors in the air are used to receive and process spread-spectrum signals in the experimental research on the acquisition performance of the FFT algorithm. The correctness of the acquisition algorithm is verified by the results of the simulation and experiments, followed by an investigation of the effects of the signal parameters and sampling frequency on the acquisition performance. The following conclusions are drawn: (1) Both lengthening the spreading spectrum code and increasing the number of intra-chip carriers can sufficiently improve the acquisition performance, but increasing the sampling frequency has a very limited improvement effect on the acquisition performance; (2) The effect of the spreading spectrum code parameters on the acquisition performance is generally dependent on the integral time Ts, which in turn is determined jointly by the length of the spreading spectrum code and the number of intra-chip carriers; (3) In the case of multipath reverberation, compared with the signal with a long spreading spectrum code and the same Ts, the signal that has a large number of intra-chip carriers and small code length is likely to cause a peak gain and a very large proportion in the width of the correlation peaks. The large proportion will lead to ambiguity in the phase acquired by the fixed threshold method. These results can provide guidance for the design and parameter selection of low frequency spread-spectrum signals. It is necessary to investigate the effect of a multipath environment on the acquisition performance of low-frequency spread-spectrum signals in future work.

Author Contributions: Conceptualization, Y.T., Q.Z. and X.L.; methodology, Y.T.; software, Y.T.; validation, Y.T. and Z.X.; Resources, W.L. and Z.X.; Experience, Y.T., X.L. and W.L.; writing—original draft preparation, Y.T.; writing—review and editing, Y.T., Q.Z., Z.X. and X.L. All authors have read and agreed to the published version of the manuscript.

Funding: This research was funded by the National Natural Science Foundation of China, grant number 52071334.

Institutional Review Board Statement: Not applicable.

Informed Consent Statement: Not applicable.

Data Availability Statement: The data present in this study are available on request from the corresponding author.

Acknowledgments: The research was supported by the National Natural Science Foundation of China (52071334). We thank the editors and the reviewers for their useful comments that improved this paper.

Conflicts of Interest: The authors declare no conflict of interest. The funders had no role in the design of the study; in the collection, analyses, or interpretation of data; in the writing of the manuscript; or in the decision to publish the results.

References

1. Tian, R.; Chi, Y. *Spread Spectrum Communication*, 2nd ed.; Qinghua University Publishing House: Beijing, China, 2014; pp. 21–29.
2. Peterson, R.L.; Borth, D.E.; Ziemer, R.E. *Introduction to Spread Spectrum Communications*, 1st ed.; Person Education: London, UK, 1995; pp. 1–32.

3. Bullock, S.R. Global Navigation Satellite System. In *Transceiver and System Design for Digital Communications*, 5th ed.; The Institution of Engineering and Technology: London, UK, 2017; Volume 13, pp. 310–325.
4. Heinrichs, G.; Rohmer, G.; Henkel, F. A fully digital direct-sequence spread-spectrum receiver architecture for GNSS applications. In Proceedings of the 2000 IEEE 6th International Symposium on Spread Spectrum Techniques and Applications, Parsippany, NJ, USA, 6–8 September 2000; Volume 512, pp. 510–514. [CrossRef]
5. Tamang, N.D.; Sur, S.N.; Bera, S.; Bera, R. A Review on Spread Spectrum Radar. *Adv. Electron. Commun. Comput.* **2018**, *1*, 653–664. [CrossRef]
6. Toru, I.; Yoshikawa, Y.; Izumi, S.; Kawaguchi, H. Subcentimeter Precision Ranging System for Moving Targets with a Doppler-Effect- Compensated Ultrasonic Direct Sequence Spread Spectrum. *IEEE Trans. Instrum. Meas.* **2020**, *70*, 1–8. [CrossRef]
7. Kumakura, K.; Suzuki, A.; Iyota, T. Code division positioning by continuous signals using spread spectrum ultrasonic waves. *Int. Conf. Indoor Position. Indoor Navig.* **2013**, 1–8. [CrossRef]
8. Paredes, J.A.; Álvarez, F.J.; Aguilera, T.; Villadangos, J.M. 3D Indoor Positioning of UAVs with Spread Spectrum Ultrasound and Time-of-Flight Cameras. *Sensors* **2017**, *18*, 89. [CrossRef]
9. Stojanovic, M.; Proarkis, J.; Rice, J.; Green, M. Spread spectrum underwater acoustic telemetry. *IEEE Ocean. Eng. Soc.* **1998**, *652*, 650–654. [CrossRef]
10. Freitag, L.; Ball, K.; Partan, J.; Koski, P.; Singh, S. Long range acoustic communications and navigation in the Arctic. *Ocean. 2015 MTS/IEEE Wash.* **2015**, 1–5. [CrossRef]
11. Zhu, M.; Wu, Y. Development of underwater acoustic communication technology. *J. Chin. Acad. Sci.* **2019**, *34*, 289–296. [CrossRef]
12. Brusin, E. Direct Sequence Spread Spectrum Signal's Demodulator Acquisition Implementation Based on Fast Fourier Transform. Part 1. Problem Statement and Solution Approach. *Proc. Telecommun. Univ.* **2022**. [CrossRef]
13. Grant, P.; Spangenberg, S.; Scott, I.; McLaughlin, S.; Povey, G.; Cruickshank, D. Doppler estimation for fast acquisition in spread spectrum communication systems. *IEEE 5th Int. Symp. Spread Spectr. Technol. Appl.* **1998**, *101*, 106–110. [CrossRef]
14. Spangenberg, S.M.; Scott, I.; McLaughlin, S.; Povey, G.J.; Cruickshank, D.G.; Grant, P.M. An FFT-Based Approach for Fast Acquisition in Spread Spectrum Communication Systems. *Wirel. Pers. Commun.* **2000**, *13*, 27–55. [CrossRef]
15. Huang, R.; Li, C.; Zhang, H.; Xie, Q. An Improved PMF-FFT Acquisition Algorithm Based on Trigonometric Polynomial Interpolation. In Proceedings of the 2022 6th International Conference on Electronic Information Technology and Computer Engineering, Xiamen, China, 21–23 October 2022. [CrossRef]
16. Ren, C. Acquisition and Tracking of GPS C/A Code in High Dynamic. Master's Thesis, Xi'an University of Science and Technology, Xi'an, China, 2020.
17. Shi, X.; Shen, Y.; Wang, Y. Fuzzy Logic Control for Doppler Search in DSSS Systems. *IEEE Trans. Fuzzy Syst.* **2019**, *28*, 2232–2243. [CrossRef]
18. Ma, X. Design and Performance Evaluation of Spread Spectrum Code for Satellite Navigation Signal. Master's Thesis, University of Chinese Academy of Sciences, Shenzhen, China, 2020. [CrossRef]
19. Mina, T.Y.; Gao, G.X. Designing Low-Correlation GPS Spreading Codes with a Natural Evolution Strategy Machine-Learning Algorithm. *J. Inst. Navig.* **2022**, *69*, 1–23. [CrossRef]
20. Sun, B.; Zheng, Z.; Zhou, Y.; Zhang, R. Research on fast acquisition algorithm of spread spectrum signal based on PMF-FFT. In Proceedings of the 2022 7th International Conference on Communication, Chengdu, China, 18–20 November 2022; pp. 291–296. [CrossRef]
21. Hussain, A.; Ahmed, A.; Magsi, H.; Soomro, J.; Bukhari, S.; Ro, J.-S. Adaptive Data Length Method for GPS Signal Acquisition in Weak to Strong Fading Conditions. *Electronics* **2021**, *10*, 1735. [CrossRef]